

Article

Modal Analysis and Experiment of a *Lycium barbarum* L. Shrub for Efficient Vibration Harvesting of Fruit

Jian Zhao ¹, Satoru Tsuchikawa ², Te Ma ², Guangrui Hu ¹, Yun Chen ¹, Zhiwei Wang ¹, Qingyu Chen ¹, Zening Gao ¹ and Jun Chen ^{1,*}

- ¹ College of Mechanical and Electronic Engineering, Northwest A&F University, Yangling, Xianyang 712100, China; 2017052634@nwsuaf.edu.cn (J.Z.); 2017050952@nwsuaf.edu.cn (G.H.); chenyun_jd@nwsuaf.edu.cn (Y.C.); zhiweiwang@nwsuaf.edu.cn (Z.W.); 1013137743@nwafu.edu.cn (Q.C.); 2019050925@nwafu.edu.cn (Z.G.)
- ² Graduate School of Bioagricultural Sciences, Nagoya University, Furo-Cho, Chikusa, Nagoya 464-8601, Japan; st3842@agr.nagoya-u.ac.jp (S.T.); mate@agr.nagoya-u.ac.jp (T.M.)
- * Correspondence: chenjun_jdxy@nwsuaf.edu.cn; Tel.: +86-29-8709-1867

Abstract: The most common harvesting method of *Lycium barbarum* L. (*L. barbarum*) is manual harvesting, resulting in low efficiency and high cost. Meanwhile, the efficiency of vibration harvesting, which is considered an efficient mechanical harvesting method, can be significantly improved if the optimized resonance frequency of the shrub can be obtained. To vibration harvest fruit efficiently, a 3D model of the shrub was established based on measurements of the shape parameters, and material mechanics models of the branches were established based on physical tests. The modal analysis of the shrub based on finite element method (FEM) simulation was performed to obtain the range of resonance frequency, and the modal experiment of the shrub using acceleration sensors and an impact hammer was conducted to obtain the accurate resonance frequency. Based on the results of the modal analysis and experiment, the optimized resonance frequency was determined to be 2 Hz. The field experiment showed that the fruit fell off when the branches were vibrated at this frequency. The results provide the design basis for the efficient vibration harvesting of *L. barbarum*.

Keywords: *L. barbarum*; modal analysis; material mechanics model; resonance frequency; FEM simulation; vibration harvesting; precision agriculture; agricultural machinery



Citation: Zhao, J.; Tsuchikawa, S.; Ma, T.; Hu, G.; Chen, Y.; Wang, Z.; Chen, Q.; Gao, Z.; Chen, J. Modal Analysis and Experiment of a *Lycium barbarum* L. Shrub for Efficient Vibration Harvesting of Fruit. *Agriculture* **2021**, *11*, 519. <https://doi.org/10.3390/agriculture11060519>

Academic Editor: Maria Gloria Lobo

Received: 29 April 2021

Accepted: 1 June 2021

Published: 3 June 2021

Publisher's Note: MDPI stays neutral with regard to jurisdictional claims in published maps and institutional affiliations.



Copyright: © 2021 by the authors. Licensee MDPI, Basel, Switzerland. This article is an open access article distributed under the terms and conditions of the Creative Commons Attribution (CC BY) license (<https://creativecommons.org/licenses/by/4.0/>).

1. Introduction

Lycium barbarum L. (*L. barbarum*) is a solanaceous *Lycium* shrub [1]. The ripe fruit contains bioactive components, e.g., *L. barbarum* polysaccharides, which help with glucose control in diabetics, immunomodulation, and so on [2]. However, mechanical harvesting of the ripe fruit has been a great challenge, and the fruit is harvested manually, resulting in low efficiency and high cost [1,3,4]. Additionally, fruit too often rots in the field without being harvested in time, resulting in economic losses. Harvesting is a major factor affecting the quality of fruit in the supply chain [5]. With the continuous expansion of *L. barbarum* acreage, labor for fruit harvesting has become increasingly scarce [1,3,6]. Therefore, it is urgent to develop harvesting machines for *L. barbarum* [1,6]. At present, some prototype *L. barbarum* harvesting machines have been developed in trials [1,3,6–15]. Based on the results of field experiments with these prototype harvesting machines, vibration harvesting was considered an efficient mechanical harvesting method [6]. The efficiency of vibration harvesting can be significantly improved if the optimized resonance frequency of the shrub can be obtained [16–19]. Therefore, it would make sense to conduct a modal analysis and experiment on the *L. barbarum* shrub. Based on the obtained optimized resonance frequency of the shrub, it is possible to design a vibration harvesting machine to harvest fruit efficiently [20]. The results are expected to provide the design basis for future research and development of efficient vibration harvesting of *L. barbarum*.

In this study, a 3D model of the shrub was established based on measurements of the shape parameters, and material mechanics models of the branches were established based on physical tests. The modal analysis of the shrub based on finite element method (FEM) simulation was performed to obtain the range of resonance frequency, and the modal experiment of the shrub using acceleration sensors and an impact hammer was conducted to obtain the accurate resonance frequency. It was expected that the fruit would fall off when the branches were vibrated at an optimized resonance frequency based on the results of the modal analysis and experiment. Such findings could provide the design basis for the efficient vibration harvesting of *L. barbarum*.

2. Materials and Methods

2.1. Establishment of the 3D Model

To provide an accurate model for the subsequent modal analysis of the *L. barbarum* shrub, it was necessary to measure the shape parameters of the shrub. In this study, the shrub had four branches, namely the main branch, primary branch, secondary branch, and fruiting branch. Each branch was simplified as a cylinder with variable diameters. ‘Ningqi 7’ was selected as the experimental variety in Zhongning in the Ningxia Hui Autonomous Region (37°22′56″ N, 105°37′21″ E) on June 18, 2019. The shrubs were 5–6 years old with a height of 0.6–1.4 m after pruning. The row spacing of the shrubs was 3 m and the shrub spacing was 1 m. The temperature was 23.4 °C, the humidity was 23.5%, and the illuminance was 428.2 Lx. A shrub was randomly selected as the measuring sample. The length of the branches was measured with a steel tape (type: AIRAJ; measurement range: 0–5 m; manufactured by Qingdao Yigou Hardware Tools Co., Ltd., Qingdao, China), the head diameter and end diameter of the branches were measured with an electronic vernier caliper (type: AIRAJ second-generation product; measurement range: 0–300 mm; precision: 0.01 mm; manufactured by Qingdao Yigou Hardware Tools Co., Ltd., Qingdao, China), and the number of the branches was determined by counting. The shape parameters of the *L. barbarum* shrub are listed in Table 1. Based on the obtained parameters, the 3D model of the *L. barbarum* shrub was established in the CATIA version-5 software and is shown in Figure 1a.

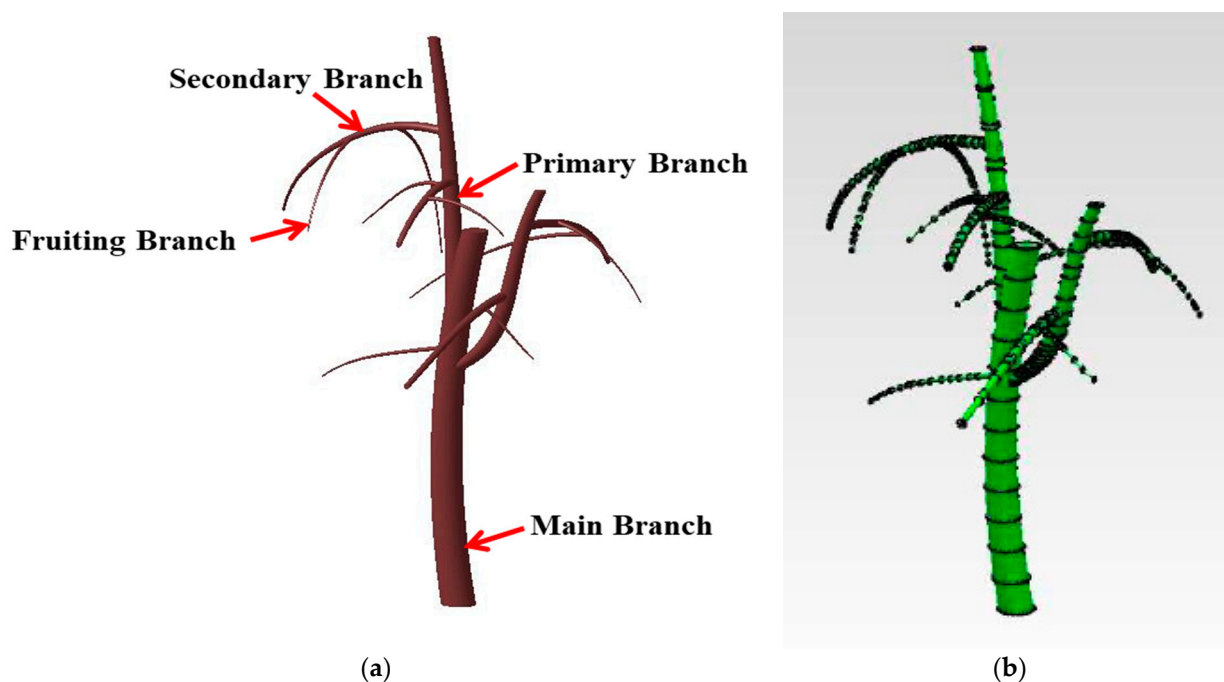


Figure 1. The 3D model of the *L. barbarum* shrub (a) and the 3D model of the *L. barbarum* shrub with reference points (b).

Table 1. The shape parameters of the *L. barbarum* shrub.

Item	The Length of the Branches (mm)	The Head Diameter of the Branches (mm)	The End Diameter of the Branches (mm)	The Number of the Branches
Main Branch	425	34.13	25.55	-
Primary Branch	235	20.03	12.86	2
Secondary Branch	340	10.45	6.89	2
Fruiting Branch	470	4.65	2.45	2

2.2. Physical Tests of the Branches Using the Universal Testing Machine

As shown in Figure 2, the property of an orthotropic material can be characterized by nine engineering constants (i.e., the radial elastic moduli E_x and E_y ; axial elastic modulus E_z ; axial shear modulus G_{xy} ; radial shear moduli G_{yz} and G_{xz} ; and Poisson's ratios u_{xy} , u_{yz} , and u_{xz}) [21]. Based on the assumption that all branches were cylinders, the branches were considered transverse isotropic [22]. Since the relationship between the nine engineering constants is described in the following five equations (Equations (1)–(5)), the number of independent engineering constants is five [21–23].

$$E_x = E_y \quad (1)$$

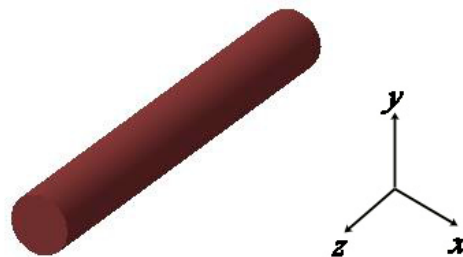
$$G_{yz} = G_{xz} \quad (2)$$

$$u_{yz} = u_{xz} \quad (3)$$

$$G_{xy} = \frac{E_x}{2(1 + u_{xy})} \quad (4)$$

$$u_{yz} < \frac{E_x}{E_z \sqrt{2u_{xy}}} \quad (5)$$

where E_x and E_y are the radial elastic moduli, MPa; E_z is the axial elastic modulus, MPa; G_{xy} is the axial shear modulus, MPa; G_{yz} and G_{xz} are the radial shear moduli, MPa; and u_{xy} , u_{yz} , and u_{xz} are the Poisson's ratios.

**Figure 2.** The simplified model of a branch.

To obtain the necessary parameters for the calculation of the engineering constants, an electronic universal testing machine (type: DDL10; max testing force: 10 kN; manufactured by Sinotest Equipment Co., Ltd., Changchun, China) was used to perform the physical tests. All physical tests were carried out in the universal testing machine laboratory of the College of Mechanical and Electronic Engineering (Northwest A&F University, Xianyang, Shaanxi, China) on 22 June 2019 at a temperature of 19.8 °C. The tests were controlled by the TestExpert.NET software. Furthermore, 1 mm min⁻¹ was selected as the test speed, and the sampling frequency was 10 Hz. Based on [13,24,25], the size of samples should meet the requirement of the following equation (Equation (6)) in the compression tests:

$$1 < \frac{L_0}{D_0} < 3 \quad (6)$$

where L_0 is the nominal length of the samples, mm, and D_0 is the nominal diameter of the samples, mm.

In addition, the cutting surface of the samples needed to be polished before the tests. After polishing the samples, the radial compression tests and axial compression tests of the branches were conducted. Based on the test method given in [26], the size of the samples should meet the requirements of the following equations (Equations (7) and (8)) in the shear tests:

$$l_0 = L + 40 \quad (7)$$

$$a = \frac{L}{2} \quad (8)$$

where l_0 is the length of the samples, mm; L is the span between the two support points, mm; and a is the length beyond the support point, mm.

Based on the diameter of the samples, the length of the samples was 80 mm, the span between the two support points was 40 mm, and the length beyond the support point was 20 mm. As shown in Figure 3, the deflection increment of the extension point could be calculated according to the following equation (Equation (9)):

$$f_1 = \frac{f_L + f_R}{2} \quad (9)$$

where f_1 is the average deflection increment of the two extension points, mm; f_L is the deflection increment of the left extension point, mm; and f_R is the deflection increment of the right extension point, mm.

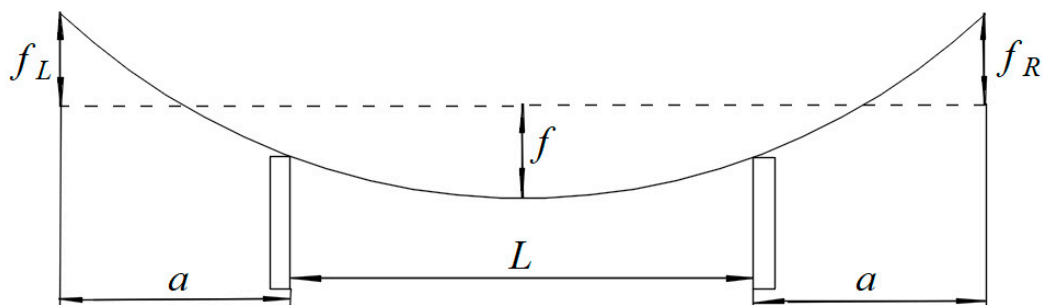


Figure 3. The measuring diagram of the shear tests.

2.3. Modal Analysis Using FEM Simulation

Numerical methods, e.g., FEM simulation, are efficient tools to predict the deformation [27]. To obtain the range of resonance frequency of the shrub, the modal analysis based on FEM simulation was performed using the Abaqus software. The 3D model of the shrub was imported in the Part module. As described in Figure 1a, the shrub was divided into four branches using the partition command. The material orientation was defined, and the material mechanics parameters of the branches as shown in Table 2 were inputted in the Property module. Since the branches were defined as the transverse isotropic, the elastic option was the engineering constants. Because frequencies obtained from the modal analysis were the key indicator, the procedure type was the linear perturbation, and the frequency was selected in this option. In order to obtain more modes, the value of the number of eigenvalues requested was determined to be 500 in the Step module. Since the root of the shrub is stationary on the ground, the boundary condition of that was the encastre in the Load module. In addition, the element library was defined as the explicit, and the geometric order was defined as the linear in the Mesh module. Furthermore, the approximate element size and maximum deviation factor were set as 4 and 0.5, respectively. Moreover, the element shape was defined as the Tet. The meshed shrub based on FEM simulation is shown in Figure 4a.

Table 2. The material mechanics parameters of the branches.

Item	The Density (kg/m ³)	The Radial Elastic Moduli E_x and E_y (MPa)	The Axial Elastic Modulus E_z (MPa)	The Axial Shear Modulus G_{xy} (MPa)	The Radial Shear Moduli G_{yz} and G_{xz} (MPa)	The Poisson's Ratio ν_{xy}	The Poisson's Ratio ν_{yz}	The Poisson's Ratio ν_{xz}
Main Branch	737.94	58.52	834.81	22.51	13.66	0.30	0.09	0.09
Primary Branch	804.29	62.15	642.66	23.91	36.91	0.30	0.12	0.12
Secondary Branch	886.02	33.07	288.91	12.72	11.80	0.30	0.15	0.15
Fruiting Branch	1021.60	65.49	498.59	25.19	6.63	0.30	0.17	0.17

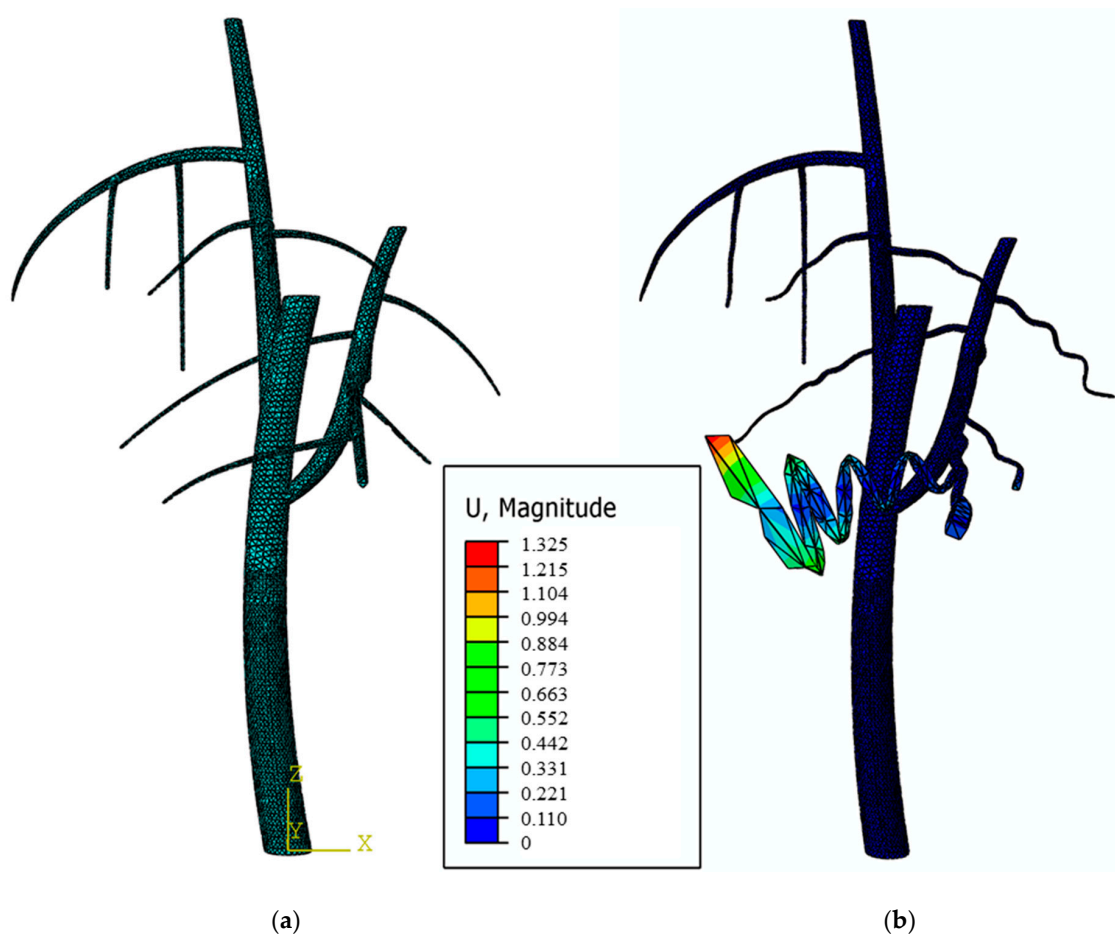


Figure 4. The meshed shrub based on FEM simulation (a) and the simulation result of the shrub at the optimized resonance frequency (b).

After meshing, 57,784 elements were generated in this simulation, and the grid was very small compared to the shrub. It was sufficient for the modal analysis of the shrub.

2.4. Modal Experiment Using Acceleration Sensors and an Impact Hammer

To obtain the accurate resonance frequency of the shrub, the modal experiment using acceleration sensors and an impact hammer was performed based on the frequencies obtained by the simulation. A dynamic signal analyzer (type: CoCo-90X; manufactured by Crystal Instruments Co., Ltd., Santa Clara, CA, USA) was used to record the signals. The global graph of the modal experiment is shown in Figure 5a. The 3D model was imported into the ME'scope software. Reference points were determined automatically in this software, and the 3D model of the *L. barbarum* shrub with the reference points is shown in Figure 1b. Therefore, three acceleration sensors (type: 356A15; manufactured

by PCB Piezotronics Inc., Depew, NY, USA) were placed at the reference points (i.e., the intersection of the main branch and primary branch, intersection of the primary branch and secondary branch, and intersection of the secondary branch and fruiting branch). The distribution of the acceleration sensors is shown in Figure 5b. The signals obtained at the above reference points were recorded by the second channel, third channel, and fourth channel, respectively. In order to obtain more accurate signals when measuring, the physical variable of the three acceleration sensors represented the acceleration; the unit was g, the sensitivity was 100.26 mV/g, the decibel parameter was 1×10^{-6} , the input pattern was IEPE, the high-pass frequency was 1 Hz, and the measurement range was 10 V.

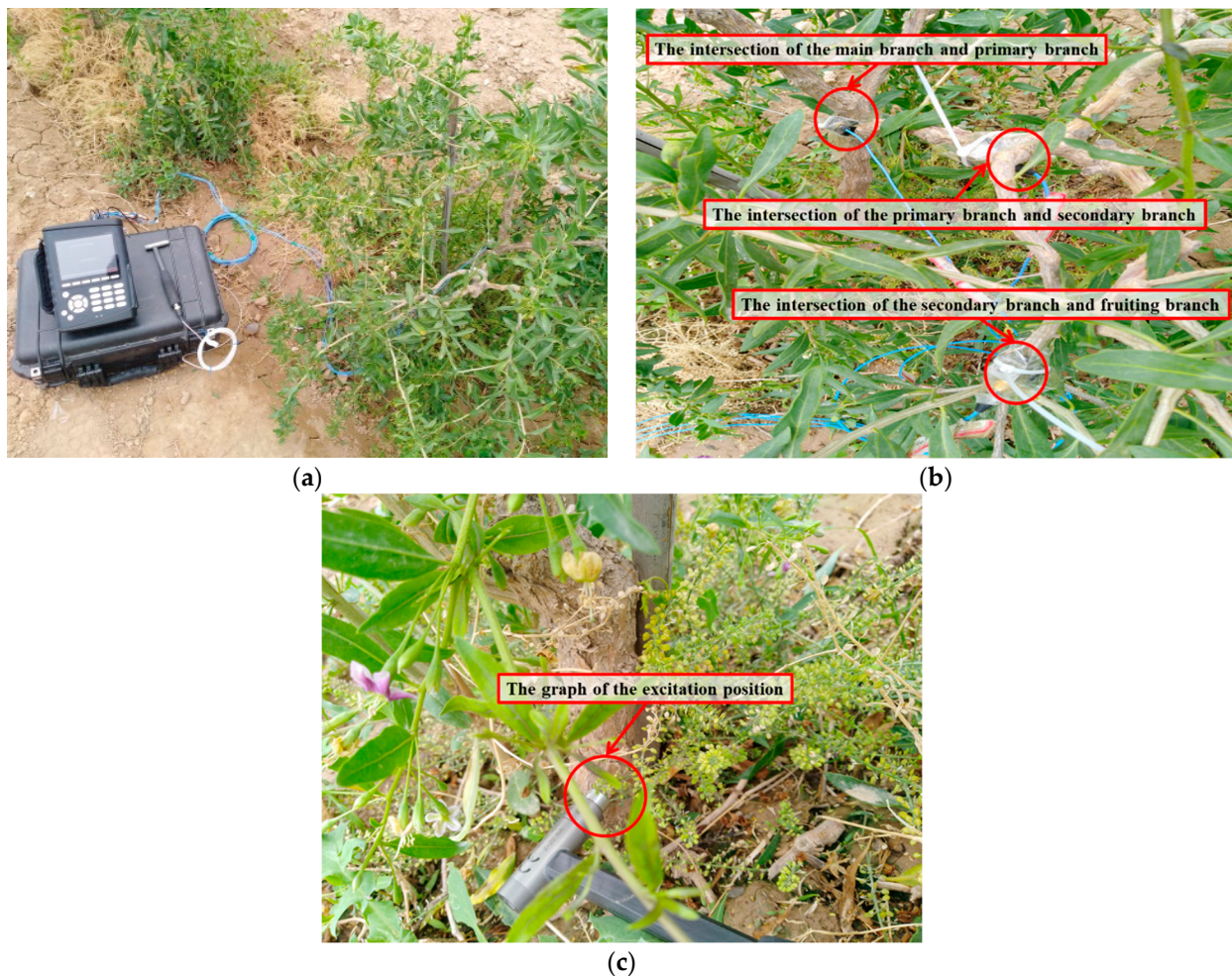


Figure 5. The modal experiment. (a) The global graph of the modal experiment; (b) the distribution of the acceleration sensors; (c) the graph of the excitation position.

In the impulse excitation test, the impact hammer (type: 086C04; manufactured by PCB Piezotronics Inc., Depew, NY, USA) hit the head of the main branch. The graph of the excitation position is shown in Figure 5c, and the signal of the impact hammer was recorded by the first channel. The physical variable of the impact hammer represented the force; the unit was N, the sensitivity was 50 mV/N, the decibel parameter was 1, the input pattern was IEPE, the high-pass frequency was 1 Hz, and the measurement range was 10 V. Moreover, the working parameters of the dynamic signal analyzer were set. The recorded data were the frequency response, the roving pattern was the response roving, the auto-increment was on, the number of increment points was 3, the sampling frequency was 12.80 kHz, the average mode was linear, the average number was 4, the window type was force-exponential, and the overlap percent was off. In addition, the type of the impact hammer was the excitation and the type of the three acceleration sensors was the response.

Furthermore, the trigger mode was a manual continuous trigger, the trigger source was the first channel, the high level was 38.0 mV, and the trigger condition was that the first channel was greater than the high level.

3. Results and Discussion

3.1. Establishment of the Material Mechanics Models

3.1.1. Density

The masses and volumes of the branches could be measured. Based on the definition of density, the densities of the branches were calculated and are listed in Table 2.

3.1.2. Elastic Modulus

The parameters of the branches in the radial compression tests are listed in Table A1. The stress and strain could be calculated based on the following equations (Equations (10) and (11)) and [27,28]:

$$\sigma = \frac{F}{A_0} \quad (10)$$

$$\varepsilon = \frac{\Delta l}{l_0} \quad (11)$$

where σ is the stress of the branches, MPa; F is the load of the tests, N; A_0 is the cross-sectional area of the samples, mm²; ε is the strain of the branches, mm·mm⁻¹; and Δl is the length change of the samples, mm.

The elastic modulus is defined as follows based on [27–29]:

$$E = \frac{\sigma}{\varepsilon} \quad (12)$$

The parameters of the branches in the axial compression tests are listed in Table A2. Based on the compression tests and [27–30], the stress–strain curves of the branches were determined. Based on Equations (10)–(12), the elastic moduli of the branches were calculated and are listed in Table 2.

3.1.3. Shear Modulus

The axial shear modulus can be calculated based on Equation (4) and the radial elastic modulus. The parameters of the branches in the shear tests are listed in Table A3, and the load–displacement curves of the branches were determined based on the shear tests. According to the test method given in [21,26], the radial shear moduli can be calculated using the following equations (Equations (13) and (14)) and are listed in Table 2:

$$U = \frac{\Delta p \cdot L}{4(f - \frac{f_1 \cdot L}{3a})} \quad (13)$$

$$G_{yz} = \frac{4U}{\pi D^2} \quad (14)$$

where U is the shear rigidity of the samples, N; Δp is the load increment in the elastic phase, N; f is the deflection increment of the central point, mm; and D is the diameter of the samples, mm.

3.1.4. Poisson's Ratio

According to [21], the Poisson's ratio ν_{xy} was assumed to be 0.3. Based on Equation (5), the Poisson's ratios of the branches were calculated; the results are listed in Table 2.

3.2. Determination of Resonance Frequency

Five hundred resonance frequencies were obtained from the simulation results in the Visualization module. The resonance frequency could be determined by combining the results of the modal analysis and experiment. Therefore, the results of the modal

experiment needed to be processed. The data of modal experiment of the shrub were inputted into the EDM software and saved in the .uff format. Then, the data in the .uff format were opened in the ME'scope software. For the intersection of the main branch and primary branch, the intersection of primary branch and secondary branch, and the intersection of secondary branch and fruiting branch, 75, 77, and 68 peaks were counted by the complex modal indicator function in the imaginary part, respectively. The frequency responses of the three intersections were also determined and are shown in Figure A1. Combined with the simulation results, the resonance of the shrub occurred when the resonance frequency was 2 Hz. The simulation result of the shrub at the optimized resonance frequency is shown in Figure 4b. The modal experiment was also conducted by the dynamic signal analyzer to reflect the resonance effect. The average mode was exponential, the average number was 32, the window type was the Hanning, the overlap percent was off, and the sampling frequency was 12.80 kHz. The acceleration signals of the three intersections were recorded by the first channel, second channel, and third channel, respectively; the results are shown in Figure A2. The settings of the three sensors were the same as the above. The resonance of the shrub at the optimized resonance frequency occurred.

3.3. Field Experiment Verification

Based on the results of the modal analysis and experiment, the optimized resonance frequency was determined to be 2 Hz. It was envisaged that the fruit could fall off when the branch was forced to vibrate and resonated at this frequency. In order to verify whether the fruit could fall off or not at this frequency, a device that could generate the frequency of 2 Hz based on the slider-crank mechanism was designed, as shown in Figure 6.

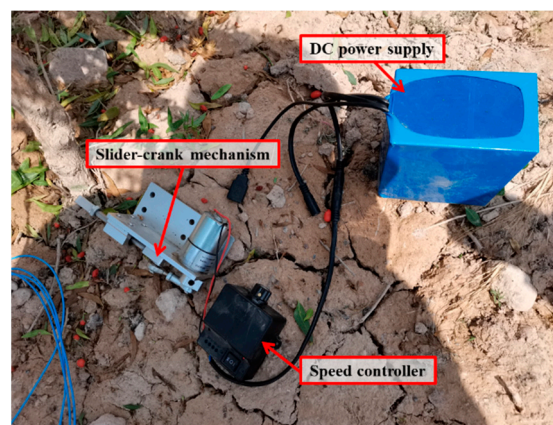


Figure 6. The device that could generate the frequency of 2 Hz.

The field experiment was completed on 4 July 2020. In order to observe the forced vibration of the branch and detachment of the fruit in detail, a high-speed camera (type: OLYMPUS i-speed TR; manufactured by Keymed (Medical & Industrial Equipment) Co., Ltd., Essex, UK) was used to record the process (Figure 7), and the recording speed was 500 fps. The red point was used to indicate the position of the fruit. As shown in Figure 7a, the branch was forced to vibrate when the device started to touch the branch at the frequency of 2 Hz. When it lasted for 0.03 s, the fruit fell off from the branch, as shown in Figure 7b.

In this field experiment, 10 groups were conducted to eliminate random errors. The results showed that all 10 fruit could fall off when the branches were forced to vibrate at the frequency of 2 Hz. In fact, the higher the vibrating frequency was, the more likely the *L. barbarum* fruit was easy to fall off quickly. This was because the higher the frequency was, the greater the energy produced. Hence, the forced vibration of *L. barbarum* fruit was more serious. However, there were three problems using too high a frequency when harvesting

L. barbarum fruit. Firstly, *L. barbarum* fruit was more severely damaged, possibly. Secondly, this also consumed more power and required the consideration of some factors, such as the structural strength when designing a high-frequency harvester. Lastly, people who used a high-frequency harvester for a long time would also experience numbness. Therefore, we wanted to find a frequency threshold at which the *L. barbarum* fruit could still fall off but the frequency would not be too high. As shown in Figure A1, a shrub had many resonant frequencies. Based on the previous thought, we chose the lowest resonant frequency. It was found that this resonant frequency was also acceptable using the simulations and experiments. Some prototype *L. barbarum* harvesting machines based on vibration as the main method were designed in the past years, as described in [1,6]. For example, Xu et al. designed a comb brush vibratory harvesting device, and Chen et al. designed a vibrating and comb brushing harvester. However, the two machines were designed combining the vibrating and comb brushing as the harvesting method and not evaluated in terms of the vibrating frequency. Zhang et al. designed an *L. barbarum* harvester by vibration mode but chose the rotational speed as the evaluation indicator [3]. Five vibrating harvesters were designed and evaluated in terms of the vibrating frequency in [8,11–13,15]. These obtained frequencies were the same order of magnitude as the frequency of 2 Hz obtained in this study. Wang et al. studied the mechanized harvesting methods of *L. barbarum* fruit and conducted an experiment by designing a vibration picking machine [31]. They vibrated the branch from a macro perspective. Meanwhile, they calculated the frequency based on the motor speed. However, under the load, the relationship between the motor speed and the frequency of the endpoint was changed. In addition, the endpoint of our device was directly acting on the joint between the branch and stem. We did not take into account the loss of energy on the branches. Therefore, it was normal that the obtained frequency was lower than their results. The frequencies obtained in these other studies were slightly higher than the obtained frequency in this study and the same order of magnitude as the frequency of 2 Hz obtained in this study. The results provide the design basis for the efficient vibration harvesting of *L. barbarum*. Furthermore, with the improvement of intelligence, the robot harvesting of *L. barbarum* was also an advanced method [32]. The obtained results also provide a theoretical basis for this method. Meanwhile, the wood properties of *L. barbarum* were important to design a harvester [33]. The obtained material mechanics parameters (i.e., the densities, elastic moduli, shear moduli, and Poisson's ratios) also provide data support for the related *L. barbarum* research. The obtained parameters in this study were the same order of magnitude as these parameters from [21,23,29].



Figure 7. The process before the vibration (a) and under the vibration (b) recorded by the high-speed camera.

4. Conclusions

In this study, a 3D model of the shrub was established based on measurements of the shape parameters, and material mechanics models of the branches were established

based on physical tests. The modal analysis of the shrub based on FEM simulation was performed to obtain the range of resonance frequency, and the modal experiment of the shrub using acceleration sensors and an impact hammer was conducted to obtain the accurate resonance frequency. The field experiment showed that the fruit fell off when the branches were vibrated at the frequency of 2 Hz based on the results of the modal analysis and experiment. Findings provided the design basis for the efficient vibration harvesting of *L. barbarum*. Because of the limitation of the number of samples, further analysis of universality will be conducted. Furthermore, an efficient vibrating harvester of *L. barbarum* will be designed based on the obtained results in the future.

Author Contributions: Conceptualization, J.Z. and J.C.; methodology, J.Z. and Y.C.; software, J.Z. and G.H.; validation, J.Z. and Z.W.; investigation, J.Z., Q.C. and Z.G.; writing—original draft preparation, J.Z.; writing—review and editing, J.C., S.T. and T.M.; visualization, J.Z.; funding acquisition, J.C. All authors have read and agreed to the published version of the manuscript.

Funding: This research and APC were funded by the National Key Research and Development Program of China, grant number 2018YFD0701102. The authors also appreciate the financial support provided by the China Scholarship Council.

Conflicts of Interest: The authors declare no conflict of interest.

Appendix A

Table A1. The parameters of the branches in the radial compression tests.

Item	The Length of the Samples l_0 (mm)	The Cross-Sectional Area of the Samples A_0 (mm ²)	The Mass of the Samples m (g)	The Radial Elastic Moduli E_x and E_y (MPa)
Main Branch	30.11	659.7101	21.448	58.5241
Primary Branch	19.66	291.4595	6.579	62.1547
Secondary Branch	9.44	81.2312	1.137	33.0742
Fruiting Branch	4.62	22.8459	0.184	65.4879

Table A2. The parameters of the branches in the axial compression tests.

Item	The Length of the Samples l_0 (mm)	The Cross-Sectional Area of the Samples A_0 (mm ²)	The Mass of the Samples m (g)	The Axial Elastic Modulus E_z (MPa)
Main Branch	38.94	580.2148	17.815	834.8138
Primary Branch	28.93	217.2073	5.515	642.6568
Secondary Branch	17.07	73.2899	1.036	288.9112
Fruiting Branch	6.88	14.7934	0.095	498.5862

Table A3. The parameters of the branches in the shear tests.

Item	The Deflection Increment of the Central Point f (mm)	The Deflection Increment of the Left Extension Point f_L (mm)	The Deflection Increment of the Right Extension Point f_R (mm)	The Diameter of the Samples D (mm)	The Axial Shear Modulus G_{xy} (MPa)	The Radial Shear Moduli G_{yz} and G_{xz} (MPa)
Main Branch	12.69	5.95	4.16	28.52	22.5093	13.6643
Primary Branch	6.63	5.29	5.98	17.17	23.9057	36.9129
Secondary Branch	5.49	4.10	3.04	7.42	12.7208	11.7980
Fruiting Branch	5.30	2.83	4.05	3.23	25.1877	6.6284

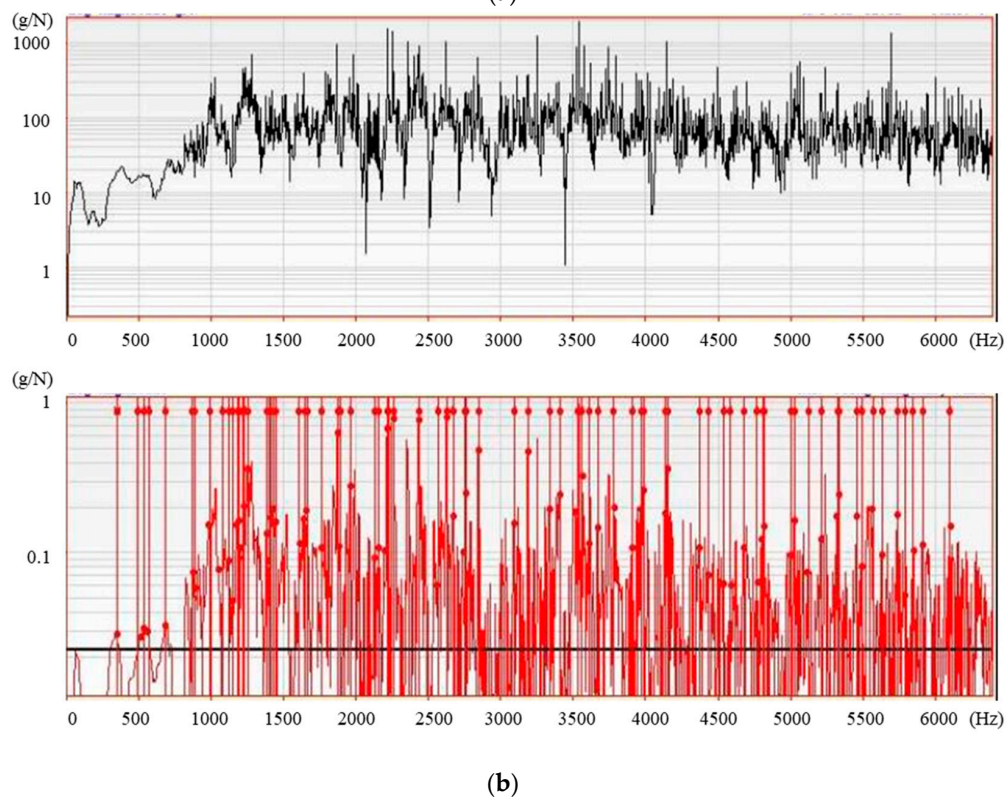
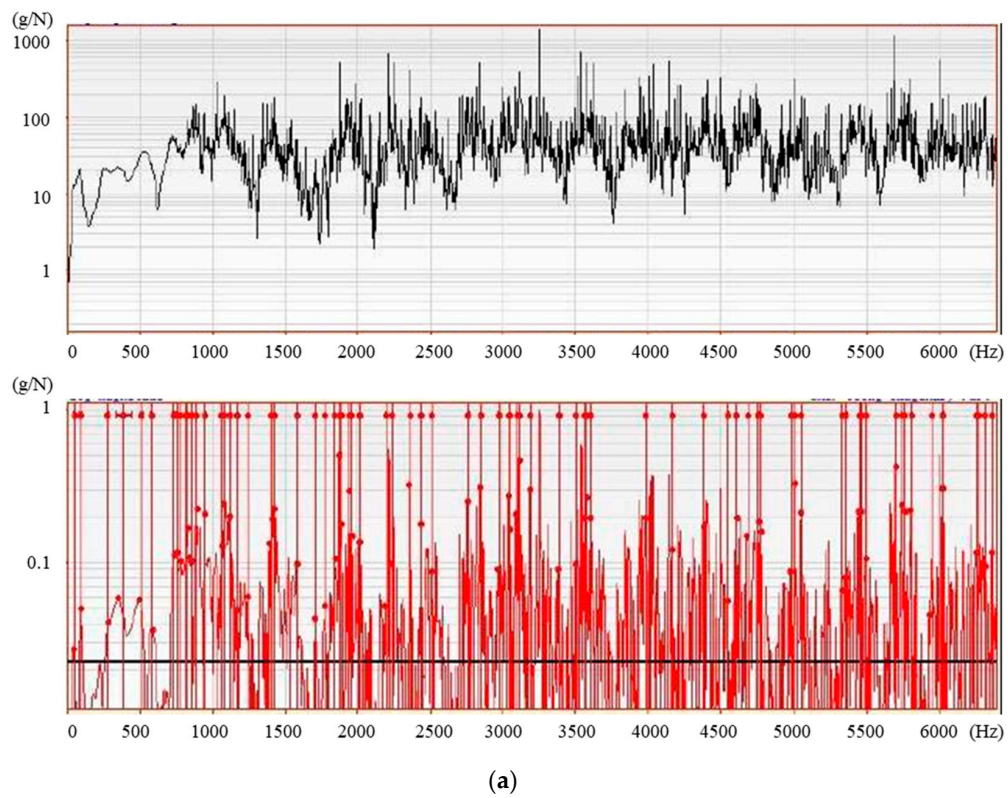


Figure A1. Cont.

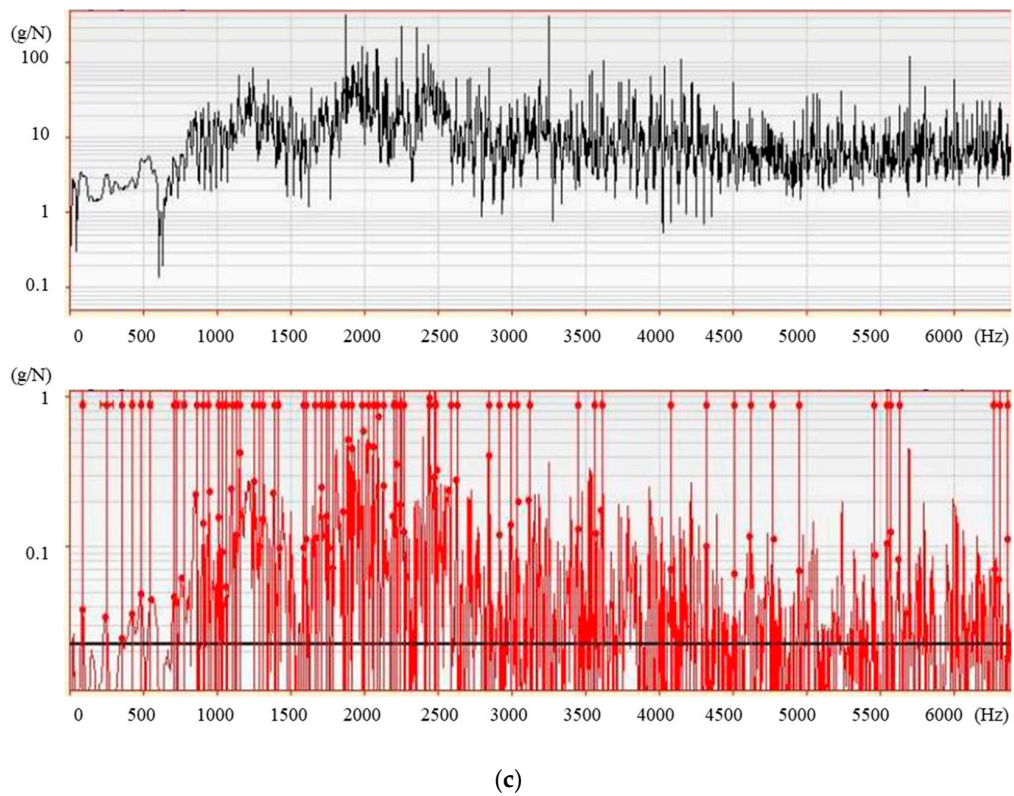


Figure A1. The frequency responses of the intersection of the main branch and primary branch (a), the intersection of the primary branch and secondary branch (b), and the intersection of the secondary branch and fruiting branch (c).

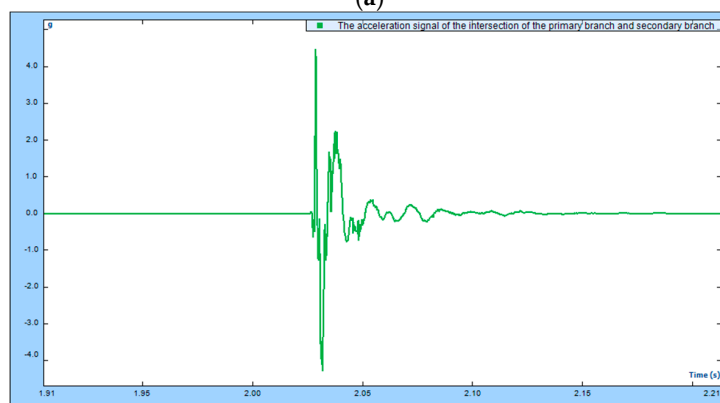
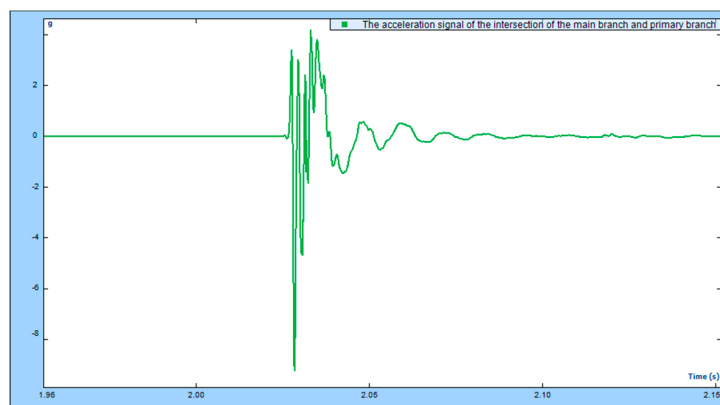
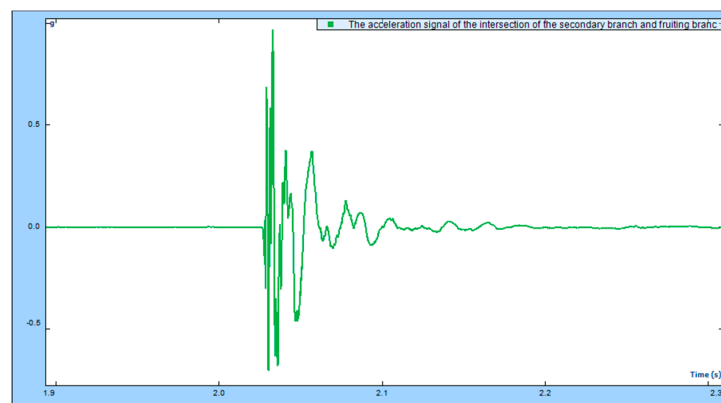


Figure A2. Cont.



(c)

Figure A2. The acceleration signals of the intersection of the main branch and primary branch (a), the intersection of the primary branch and secondary branch (b), and the intersection of the secondary branch and fruiting branch (c).

References

- Xu, L.; Chen, J.; Wu, G.; Yuan, Q.; Ma, S.; Yu, C.; Duan, Z.; Xing, J.; Liu, X. Design and operating parameter optimization of comb brush vibratory harvesting device for wolfberry. *Trans. CSAE* **2018**, *34*, 75–82. [[CrossRef](#)]
- Amagase, H.; Farnsworth, N.R. A review of botanical characteristics, phytochemistry, clinical relevance in efficacy and safety of *Lycium barbarum* fruit (Goji). *Food Res. Int.* **2011**, *44*, 1702–1717. [[CrossRef](#)]
- Zhang, Z.; Xiao, H.; Ding, W.; Mei, S. Mechanism simulation analysis and prototype experiment of *Lycium barbarum* harvest by vibration mode. *Trans. CSAE* **2015**, *31*, 20–28. [[CrossRef](#)]
- Zhao, J.; Sugirbay, A.; Liu, F.; Chen, Y.; Hu, G.; Zhang, E.; Chen, J. Parameter optimization of winnowing equipment for machineharvested *Lycium barbarum* L. *Span. J. Agric. Res.* **2019**, *17*, e0203. [[CrossRef](#)]
- Rodjanatham, T.; Rabgyal, T. Quality assurance of international fruit supply chains via techno-management. *Agriculture* **2020**, *10*, 107. [[CrossRef](#)]
- Chen, J.; Zhao, J.; Chen, Y.; Bu, L.; Hu, G.; Zhang, E. Design and experiment on vibrating and comb brushing harvester for *Lycium barbarum*. *Trans. CSAM* **2019**, *50*, 152–161. [[CrossRef](#)]
- So, J.D. Vibration characteristics of boxthorn (*Lycium chinense* Mill) branches. *Appl. Eng. Agric.* **2001**, *17*, 755–760. [[CrossRef](#)]
- So, J.D. Vibratory harvesting machine for boxthorn (*Lycium chinense* Mill) berries. *Trans. ASAE* **2003**, *46*, 211–221. [[CrossRef](#)]
- Wang, Y.; Chen, Y.; Han, B.; Chen, J. Research on laws of wolfberry dropping based on high-speed camera. *J. Agric. Mech. Res.* **2018**, *40*, 166–170. [[CrossRef](#)]
- Zhang, W.; Li, Z.; Tan, Y.; Li, W. Optimal design and experiment on variable pacing combing brush picking device for *Lycium barbarum*. *Trans. CSAM* **2018**, *49*, 83–90. [[CrossRef](#)]
- Zhang, W.; Zhang, M.; Zhang, J.; Li, W. Design and experiment of vibrating wolfberry harvester. *Trans. CSAM* **2018**, *49*, 97–102. [[CrossRef](#)]
- Zhao, J.; Chen, Y.; Wang, Y.; Chen, J. Experimental research on parameter optimization of portable vibrating and harvesting device of Chinese wolfberry. *J. Agric. Mech. Res.* **2019**, *41*, 176–182. [[CrossRef](#)]
- Wang, Y. Research on Key Technology of Wolfberry Vibration Harvest. Master's Thesis, Northwest A&F University, Xianyang, China, 2018.
- Zhou, B.; He, J. Design of simulate hand wolfberry picking machine. *Trans. CSAE* **2010**, *26* (Suppl. S1), 13–17. [[CrossRef](#)]
- He, M.; Kan, Z.; Li, C.; Wang, L.; Yang, L.; Wang, Z. Mechanism analysis and experiment on vibration harvesting of wolfberry. *Trans. CSAE* **2017**, *33*, 47–53. [[CrossRef](#)]
- Láng, Z. A fruit tree stability model for static and dynamic loading. *Biosyst. Eng.* **2003**, *85*, 461–466. [[CrossRef](#)]
- Horvath, E.; Sitkei, G. Damping properties of plum trees shaken at their trunks. *Trans. ASAE* **2005**, *48*, 19–25. [[CrossRef](#)]
- Láng, Z. Dynamic modelling structure of a fruit tree for inertial shaker system design. *Biosyst. Eng.* **2006**, *93*, 35–44. [[CrossRef](#)]
- Láng, Z. A one degree of freedom damped fruit tree model. *Trans. ASABE* **2008**, *51*, 823–829. [[CrossRef](#)]
- Sargent, S.A.; Takeda, F.; Williamson, J.G.; Berry, A.D. Harvest of southern highbush blueberry with a modified, over-the-row mechanical harvester: Use of handheld shakers and soft catch surfaces. *Agriculture* **2020**, *10*, 4. [[CrossRef](#)]
- Shen, C.; Li, X.; Tian, K.; Zhang, B.; Huang, J.; Chen, Q. Experimental analysis on mechanical model of ramie stalk. *Trans. CSAE* **2015**, *31*, 26–33. [[CrossRef](#)]
- Wang, Y. *Abaqus Analysis User's Guide: Materials Volume*, 1st ed.; China Machine Press: Beijing, China, 2018; pp. 27–28.
- Shi, N. Peeling Method of Cotton Stalk and Development of Rubbing Peeling Machine. Ph.D. Thesis, Northwest A&F University, Xianyang, China, 2018.
- Wu, J.; Huang, Y.; Wang, Y.; Wang, W. Study on axial compression properties of cotton stalks. *J. Agric. Mech. Res.* **2004**, *26*, 148–149, 152. [[CrossRef](#)]

25. Wang, Y.; Su, P. Research of mechanics characteristics for cotton stalks compression. *J. Agric. Mech. Res.* **2006**, *28*, 171–172. [[CrossRef](#)]
26. The State General Administration of Quality Supervision, Inspection and Quarantine of the People's Republic of China; China National Standardization Administration Commission. *Test Method for Flexural Properties of Sandwich Constructions*; National Standards of the People's Republic of China: Beijing, China, 2005; pp. 1–9.
27. Zhao, J.; Sugirbay, A.; Chen, Y.; Zhang, S.; Liu, F.; Bu, L.; Chen, Y.; Wang, Z.; Chen, J. FEM explicit dynamics simulation and NIR hyperspectral reflectance imaging for determination of impact bruises of *Lycium barbarum* L. *Postharvest Biol. Technol.* **2019**, *155*, 102–110. [[CrossRef](#)]
28. Celik, H.K. Determination of bruise susceptibility of pears (Ankara variety) to impact load by means of FEM-based explicit dynamics simulation. *Postharvest Biol. Technol.* **2017**, *128*, 83–97. [[CrossRef](#)]
29. Shen, C.; Chen, Q.; Li, X.; Zhang, B.; Huang, J.; Tian, K. Test and analysis of axial compressive mechanical properties for ramie stalk. *Acta Agric. Univ. Zhejiangensis* **2016**, *28*, 688–692. [[CrossRef](#)]
30. Viet, D.D.; Ma, T.; Inagaki, T.; Kim, N.T.; Chi, N.Q.; Tsuchikawa, S. Physical and mechanical properties of fast growing polyploid Acacia hybrids (*A. auriculiformis* × *A. mangium*) from Vietnam. *Forests* **2020**, *11*, 717. [[CrossRef](#)]
31. Wang, J.; Mei, S.; Xiao, H.; Zhao, Y.; Zhou, H. Research on mechanized harvesting methods of *Lycium barbarum* fruit. *IFAC PapersOnLine* **2018**, *51*, 223–226. [[CrossRef](#)]
32. Chen, Y.; Wang, Y.; Zhao, J.; Chen, J. Recognition of the position of Chinese wolfberry branches under the artificial background. *IFAC PapersOnLine* **2018**, *51*, 321–325. [[CrossRef](#)]
33. Zhao, J.; Ma, T.; Inagaki, T.; Chen, Q.; Gao, Z.; Sun, L.; Cai, H.; Chen, C.; Li, C.; Zhang, S.; et al. Finite element method simulations and experiments of detachments of *Lycium barbarum* L. *Forests* **2021**, *12*, 699. [[CrossRef](#)]